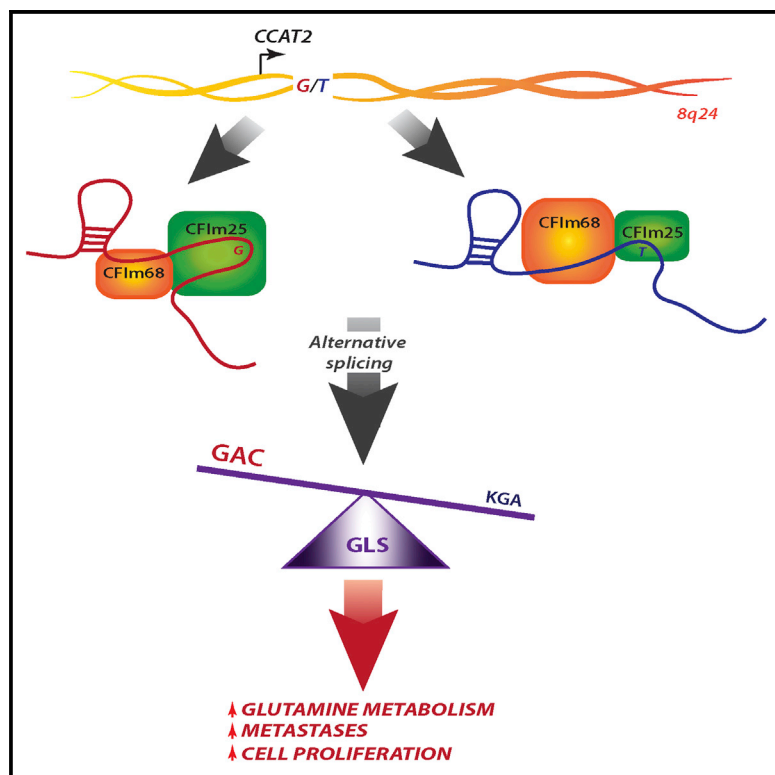


Molecular Cell

Allele-Specific Reprogramming of Cancer Metabolism by the Long Non-coding RNA CCAT2

Graphical Abstract



Authors

Roxana S. Redis, Luz E. Vela, Weiqin Lu, ..., Andre L.B. Ambrosio, Sandra M. Gomes Dias, George A. Calin

Correspondence

gcalin@mdanderson.org

In Brief

Redis et al. report that the two alleles of the lncRNA, CCAT2, induce distinct metabolic phenotypes. By interacting with the CFI complex with allele-specific affinities, CCAT2 regulates the alternative splicing of GLS, resulting in the preferential expression of the more aggressive splice isoform.

Highlights

- The lncRNA CCAT2 reprograms energy metabolism in an allele-specific manner
- CCAT2 alleles bind the CFI complex with distinct affinities
- CCAT2-CFI-GLS interaction regulates the alternative splicing of GLS
- This regulation axis is present in 61% of analyzed CRC cases



Allele-Specific Reprogramming of Cancer Metabolism by the Long Non-coding RNA CCAT2

Roxana S. Redis,¹ Luz E. Vela,² Weiqin Lu,^{3,4} Juliana Ferreira de Oliveira,⁵ Cristina Ivan,⁶ Cristian Rodriguez-Aguayo,¹ Douglas Adamoski,⁵ Barbara Pasculli,¹ Ayumu Taguchi,³ Yunyun Chen,⁸ Agustin F. Fernandez,⁹ Luis Valledor,¹⁰ Katrien Van Roosbroeck,¹ Samuel Chang,¹ Maitri Shah,¹ Garrett Kinnebrew,¹¹ Leng Han,¹² Yaser Atlasi,^{13,22} Lawrence H. Cheung,¹ Gilbert Y. Huang,¹ Paloma Monroig,¹ Marc S. Ramirez,¹⁴ Tina Catela Ivkovic,^{1,15} Long Van,² Hui Ling,¹ Roberta Gafà,¹⁶ Sanja Kapitanovic,¹⁵ Giovanni Lanza,¹⁶ James A. Bankson,¹⁴ Peng Huang,³ Stephen Y. Lai,⁸ Robert C. Bast,¹ Michael G. Rosenblum,¹ Milan Radovich,¹¹ Mircea Ivan,¹⁷ Geoffrey Bartholomeusz,¹ Han Liang,¹⁸ Mario F. Fraga,¹⁹ William R. Widger,² Samir Hanash,⁷ Ioana Berindan-Neagoe,^{1,20,21} Gabriel Lopez-Berestein,^{1,6} Andre L.B. Ambrosio,⁵ Sandra M. Gomes Dias,⁵ and George A. Calin^{1,6,*}

¹Department of Experimental Therapeutics, The University of Texas MD Anderson Cancer Center, Houston, TX 77030, USA

²Department of Biology & Biochemistry, University of Houston, Houston, TX 77204, USA

³Department of Translational Molecular Pathology, The University of Texas MD Anderson Cancer Center, Houston, TX 77030, USA

⁴Department of Gastrointestinal Medical Oncology, The University of Texas MD Anderson Cancer Center, Houston, TX 77030, USA

⁵Laboratório Nacional de Biociências, Centro Nacional de Pesquisa em Energia e Materiais, Campinas 13083-100, Brazil

⁶Center for RNA Interference and Non-coding RNAs, The University of Texas MD Anderson Cancer Center, Houston, TX 77030, USA

⁷Department of Clinical Cancer Prevention, The University of Texas MD Anderson Cancer Center, Houston, TX 77030, USA

⁸Department of Head & Neck Surgery, The University of Texas MD Anderson Cancer Center, Houston, TX 77030, USA

⁹Cancer Epigenetics Laboratory, Institute of Oncology of Asturias (IUOPA), HUCA, Universidad de Oviedo, Oviedo 33006, Spain

¹⁰Department of Organisms and Systems Biology, University of Oviedo, Oviedo 33006, Spain

¹¹Department of Surgery, Medical and Molecular Genetics, Indiana University School of Medicine, Indianapolis, IN 46202, USA

¹²Department of Biochemistry and Molecular Biology, The University of Texas Health Science Center at Houston McGovern Medical School, Houston, TX 77030, USA

¹³Department of Pathology, Josephine Nefkens Institute, Erasmus Medical Center, Rotterdam 3015, the Netherlands

¹⁴Department of Imaging Physics, Division of Diagnostic Imaging, The University of Texas MD Anderson Cancer Center, Houston, TX 77030, USA

¹⁵Laboratory for Personalized Medicine, Division of Molecular Medicine, Ruder Boskovic Institute, Zagreb 10000, Croatia

¹⁶Department of Morphology, Surgery and Experimental Medicine, University of Ferrara, Ferrara 44121, Italy

¹⁷Department of Medicine, Department of Microbiology and Immunology, Indiana University School of Medicine, Indianapolis, IN 46202, USA

¹⁸Department of Bioinformatics and Computational Biology, The University of Texas MD Anderson Cancer Center, Houston, TX 77030, USA

¹⁹Nanomaterials and Nanotechnology Research Center (CINN-CSIC), Asturias 33424, Spain

²⁰Research Center for Functional Genomics, Biomedicine and Translational Medicine, University of Medicine and Pharmacy Iuliu Hatieganu, Cluj-Napoca 400012, Romania

²¹Department of Functional Genomics, The Oncology Institute, Cluj-Napoca 400015, Romania

²²Present address: Radboud Institute for Molecular Life Sciences (RIMLS) Department of Molecular Biology, Nijmegen 6525, the Netherlands

*Correspondence: gcalin@mdanderson.org

<http://dx.doi.org/10.1016/j.molcel.2016.01.015>

SUMMARY

Altered energy metabolism is a cancer hallmark as malignant cells tailor their metabolic pathways to meet their energy requirements. Glucose and glutamine are the major nutrients that fuel cellular metabolism, and the pathways utilizing these nutrients are often altered in cancer. Here, we show that the long ncRNA *CCAT2*, located at the 8q24 amplicon on cancer risk-associated rs6983267 SNP, regulates cancer metabolism in vitro and in vivo in an allele-specific manner by binding the Cleavage Factor I (CFIm) complex with distinct affinities for the two subunits (CFIm25 and CFIm68). The *CCAT2* interaction with the CFIm complex fine-tunes the alternative splicing of *Glutaminase (GLS)* by selecting the poly(A) site in intron 14 of the precursor mRNA. These

findings uncover a complex, allele-specific regulatory mechanism of cancer metabolism orchestrated by the two alleles of a long ncRNA.

INTRODUCTION

Long non-coding RNAs (lncRNAs) form the largest part of the mammalian non-coding transcriptome (Mercer et al., 2009) and are generally expressed in a developmental-, tissue-, or disease-stage-specific manner, which makes them attractive therapeutic targets (Ling et al., 2013a). Although the underlying molecular mechanisms are not yet entirely understood, lncRNAs control gene expression at various levels including chromatin modification and transcriptional and post-transcriptional processing (Wilusz et al., 2009).

The revival of Warburg's theory of cancer (Warburg et al., 1924), complemented with novel discoveries in the field, has

promoted cellular metabolism as an essential molecular mechanism for driving malignant transformation and progression (Borouhgs and DeBerardinis, 2015). Various studies have exposed the fine interplay between metabolic pathways orchestrated by protein-coding oncogenes and tumor suppressor genes (Chen and Russo, 2012) and, more recently, by ncRNAs (miRNAs and lncRNAs) (Gao et al., 2009; Yang et al., 2014). Glutamine, one of the essential nutrients, is deaminated by *Glutaminase* (*GLS*) to produce glutamate, which further serves as substrate for a variety of metabolic pathways (e.g., tricarboxylic cycle, TCA). Glutamine metabolism is modulated by MYC via miR-23a/b in prostate cancer and B cell lymphoma (Gao et al., 2009) and by NF- κ B p65 subunit also through miR-23a downregulation in leukemic cells (Rathore et al., 2012; Wang et al., 2010b).

Colon Cancer-Associated Transcript 2 (*CCAT2*), a lncRNA that spans the highly conserved 8q24 region harboring the rs6983267 SNP (Ling et al., 2013b; Redis et al., 2013), is associated with increased risk for various types of cancer (Tomlinson et al., 2007; Tuupainen et al., 2009) and is specifically overexpressed in the microsatellite stable colorectal cancer (CRC MSS). The two alleles of the rs6983267 SNP present in the general population have been shown to render distinct risks of CRC; namely, the G allele was associated with greater predisposition to CRC than the T allele (Tomlinson et al., 2007). *CCAT2* induces chromosomal instability and metastases (Ling et al., 2013b) and regulates the expression levels of MYC oncogene, known to coordinate multiple molecular pathways supporting cell proliferation, metastases and cancer metabolism (Carroll et al., 2015; Stine et al., 2015). However, it is not clear how the two alleles are specifically involved in the malignant process. In this study, we demonstrate that the lncRNA, *CCAT2*, modulates cellular energy metabolism in an allele-specific manner by interacting with the Cleavage Factor I (CFIm) complex to regulate the alternative splicing of *GLS*.

RESULTS

CCAT2 Modulates Energy Metabolism in an Allele-Specific Manner In Vitro and In Vivo

We observed an unexpected change in the color of the media of in vitro grown cells when modulating the expression of *CCAT2* that suggested a possible shift in the energy metabolism consequent to *CCAT2* expression. We tested this hypothesis by measuring metabolic parameters in HCT116 colon cancer cells that stably overexpress *CCAT2* (OC1 and OC3) (Ling et al., 2013b) versus control cells and observed a significant and reproducible increase in glucose uptake, lactate secretion and oxygen consumption in the *CCAT2*-overexpressing clones (Figure 1A). These results were further confirmed in KM12SM cells with *CCAT2* downregulated expression (Figure 1B). Moreover, we explored whether these metabolic changes were occurring in vivo as well by injecting HCT116 *CCAT2*-overexpressing cells and control cells subcutaneously into nude mice and subjecting them to hyperpolarized magnetic resonance imaging (HP-MRI). We detected a significant increase in the flux of hyperpolarized [$1\text{-}^{13}\text{C}$]pyruvate to [$1\text{-}^{13}\text{C}$]lactate for the xenograft tumors derived from the *CCAT2*-overexpressing cells compared to the tumors derived from control cells (Figures S1A and S1B), consistent

with our in vitro findings. These findings confirm that *CCAT2* alters metabolism, boosting glycolysis and cellular respiration. The coexistence of increased glycolysis with increased respiration, in highly proliferative cells, translates into enhanced anaplerotic reactions that replenish the TCA cycle intermediates (Ward and Thompson, 2012). Since glutamine is the main source for replenishing the intermediates of the TCA cycle, we measured the intra- and extracellular glutamate concentration, as well as the glutamine uptake in HCT116 cells with *CCAT2* overexpression and control cells. We found higher levels of both intra- and extracellular glutamate corresponding to higher levels of *CCAT2* (Figures S1C and S1D), suggesting *CCAT2* is boosting glutamine metabolism (glutaminolysis). Surprisingly, the glutamine uptake was not significantly different between the three clones (Figure S1D), implying the higher glutamate is not due to increased glutamine consumption. Therefore, we measured the enzymatic activity of GLS, the rate-limiting enzyme of glutaminolysis, in the whole lysate of the same cells and detected significantly higher activity in the cells with increased *CCAT2* expression (Figure S1F). In addition, both metabolic pathways (glycolysis and glutaminolysis) have been shown to be regulated by many factors, including the MYC oncogene (Carroll et al., 2015; Stine et al., 2015), a target of *CCAT2* by our previous report (Ling et al., 2013b).

We next explored whether the rs6983267 SNP influences these metabolic changes and assessed the glucose and glutamine uptake, oxygen consumption, lactate secretion, and intra- and extracellular glutamate concentration in HCT116 stably overexpressing either the G or the T allele of *CCAT2* and control HCT116 cells. Interestingly, we found on one hand higher glucose uptake and secreted glutamate in both G and T allele cells compared to control cells, while on the other hand we observed significant differences in lactate secretion, oxygen consumption, and intracellular glutamate production between the alleles (Figures 1C and S1E). Moreover, the glutamine consumption was not significantly different between the clones, similar to our previous results (Figure S1E). Consequently, we measured GLS enzymatic activity in these cells and observed that both *CCAT2* alleles induced a remarkable increase in activity compared to control, but the cells overexpressing the G allele displayed a significantly higher enzymatic activity compared to the T allele-overexpressing cells (Figure 1D). We also analyzed by mass spectroscopy the metabolites obtained from in vitro culturing of the HCT116 *CCAT2* G or T allele and control cells and from in vivo xenografted tumors derived from subcutaneous injection of the same cells. We observed contrasting distribution patterns when performing partial least squares discriminant analysis (PLS-DA) for both the in vitro (Figure 1E) and in vivo analyses (Figure 1F), and similarly for the principal component analysis (PCA) (Figures S1G and S1H). We detected 85.04% (in vitro) and 59.55% (in vivo) of metabolic pathways upregulated by *CCAT2* G allele compared to the T allele (Figure S1I, Table S1B). We then compared the pathway analysis for both datasets and identified 40 common pathways for the G allele and five common pathways for the T allele (Figure S1J). For these pathways, metabolic cluster distribution of differentially accumulated compounds revealed a significant overall enhancement of metabolic pathways related to glucose metabolism, TCA cycle, and glutamine metabolism for the G allele cells compared to the T allele cells (Tables S1A and S1B). We

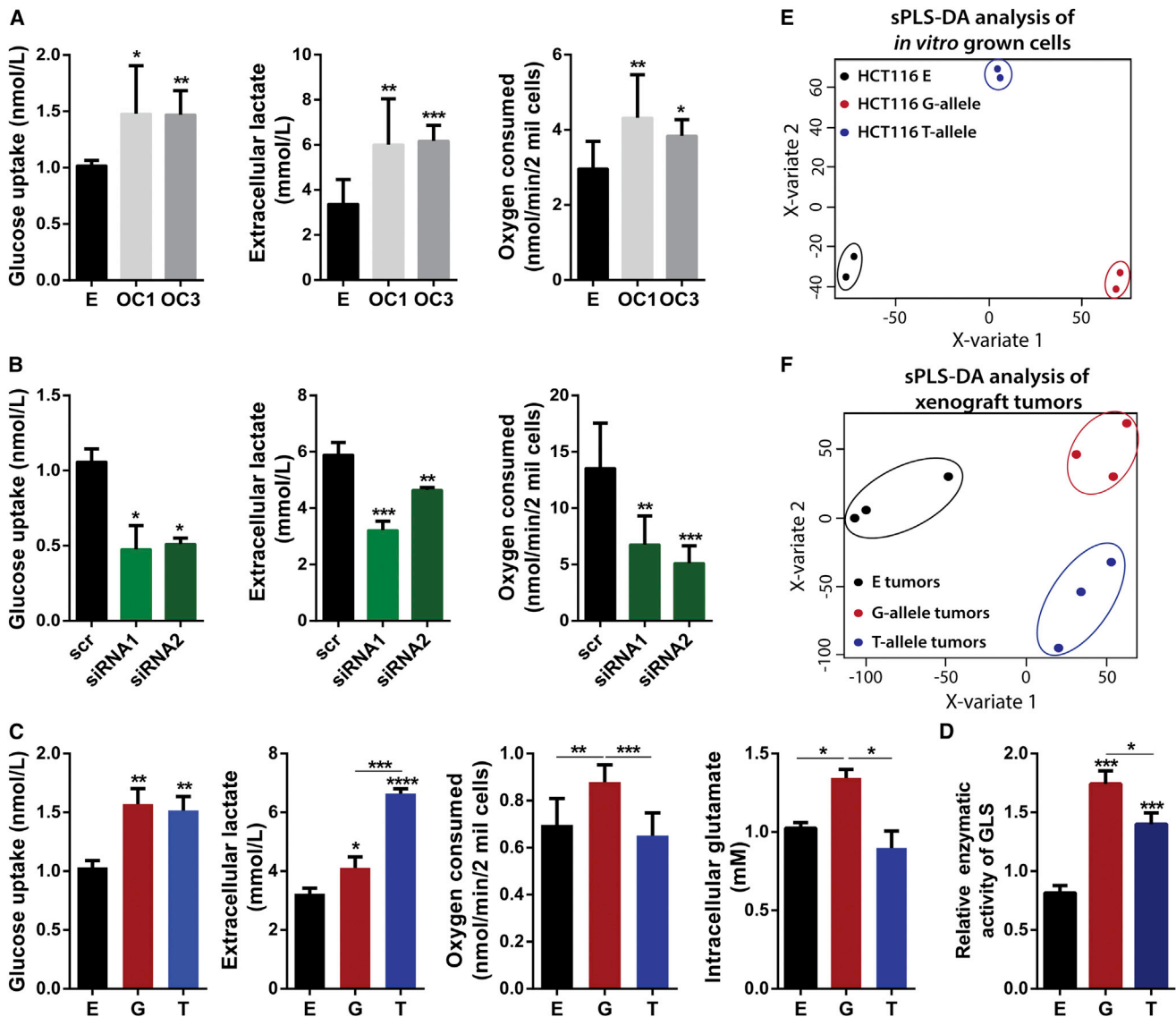


Figure 1. CCA2 Regulates Cancer Metabolism In Vitro and In Vivo

(A) Glucose uptake, lactate production, and oxygen consumption assays in HCT116 stable clones (E: empty control vector; OC1 and OC3: CCA2-overexpressing, GG genotype).

(B) Glucose uptake, lactate production, and oxygen consumption assays in KM12SM cells with CCA2 downregulation (GT genotype).

(C) Whole-cell lysate *Glutaminase* activity measured in HCT116 CCA2-overexpressing G or T allele and control cells.

(D) Partial least-squares discriminant analysis (sPLS-DA) of HCT116 cells stably overexpressing CCA2 with either G or T alleles, and control cells (E, empty vector) in vitro allowed an adequate classification of the different cell lines according to its metabolome. sPLS-DA algorithm allows the classification of the samples based on the different abundances of each metabolite trying to find the maximum covariance between treatments and metabolome, in this way finding the most important metabolites for explaining the different effects of the treatments.

(E) Xenograft tumors derived from the same cell lines were also correctly classified by sPLS-DA analysis.

Results are presented as normalized mean values \pm SD. See also Figure S1 and Table S1.

evaluated the expression of MYC between the HCT116 CCA2 G and T allele cells but did not find impressive differences, consistent with our previous findings (Ling et al., 2013b) (Figure S2A). These results imply that in cells with high CCA2 expression, MYC activates energy metabolism in a general fashion; however, the fine-tuning of distinct metabolic pathways may occur through MYC-independent, but SNP-dependent, mechanisms.

We therefore decided to direct our efforts toward exploring the CCA2 MYC-independent mechanism of regulation.

CCA2 Regulates the Expression of GLS Isoforms

Our group has previously shown that CCA2 induces chromosomal instability, a process highly reliant on the supply of nucleotides (Bester et al., 2011) and intimately linked to glutamine

metabolism (Jeong et al., 2013). Further supported by the metabolic data, we directed our focus toward pathways metabolizing glutamine. We first assessed the protein expression of the two alternative splicing isoforms of *GLS*, KGA (glutaminase kidney isoform) and GAC (glutaminase isoform C) as a function of *CCAT2*. We used specific antibodies for each isoform (recognizing the distinct C termini) (Cassago et al., 2012) and/or a common antibody, recognizing the N terminus shared by the two isoforms, depending on the cell line. Although the two isoforms share the same active site, GAC has a higher catalytic activity than KGA and therefore may be more relevant for replenishing intermediates of the TCA cycle (Cassago et al., 2012; Le et al., 2012). While for GAC we observed an increase in protein expression in the HCT116 *CCAT2*-overexpressing cells with both antibodies, for KGA the protein expression presented an inconsistent variation with *CCAT2* upregulation (Figures 2A, S2B, and S2C). Analogously, the mRNA expression pattern for GAC and KGA reflected the protein expression (Figure 2B). Moreover, downregulation of *CCAT2* in KM12SM cells reduced GAC protein expression with 34% and 26%, respectively (Figures 2C, S2D, and S2E), whereas KGA protein expression was either unaltered or slightly increased (Figures 2C, S2D, and S2E). Similar results were obtained when measuring the mRNA expression of the two isoforms in the same cellular model (Figure S2F). Interestingly, when we evaluated the expression of the two isoforms in the HCT116 cells overexpressing the *CCAT2* G or T allele and control cells at both the mRNA and protein levels, we found unanimously higher expression of GAC when *CCAT2* G allele is upregulated (Figures 2D and S2G–S2I). However, changes in the KGA mRNA expression pattern did not concur with the protein expression (Figures 2D and S2G–S2I). The discordance observed for the KGA isoform is probably due to the regulation by the MYC-miR-23 axis (Gao et al., 2009; additional data available from authors upon request). These results alluded to the idea that *CCAT2* may preferentially induce the splicing of the GAC isoform. To determine this, we cloned the intron 14 of *GLS* precursor mRNA, known to encompass the alternative splicing site, in the RG6 bichromatic fluorescent reporter (Orengo et al., 2006). If the splicing machinery binds to the intron 14, it induces the splicing of a EGFP-tagged protein, which is the equivalent of GAC; otherwise, a dsRED-tagged protein will be produced, which is the equivalent of KGA (Figure S2J). We transfected the HCT116 control and *CCAT2*-overexpressing cells with the fluorescent reporter and determined the ratio between the expression levels of EGFP and dsRED fluorescence using the VECTRA automated imaging system. Although the EGFP-tagged protein, GAC-equivalent, was predominant in all models, we observed a 50% significantly higher EGFP/dsRED ratio in the *CCAT2*-overexpressing cells, corresponding to 50% more alternative splicing events (Figure 2E). Similar results were obtained when cells were analyzed by flow cytometry (Table S2). Moreover, when we compared the alternative splicing events occurring in the G and T alleles, using the RG6 reporter, we found significantly higher EGFP/dsRED ratio for the *CCAT2* G allele compared to the *CCAT2* T allele (Figure 2F and Table S2). Altogether, these data demonstrate that the *CCAT2* G allele is more efficient in boosting the alternative splicing of GAC isoform.

CFIm25 Governs the Switch between *GLS* Splicing Isoforms

To elucidate the underlying mechanism of *CCAT2*-induced regulation of the *GLS* alternative splicing, we introduced the MS2 tag (24 repeats) into vectors containing either the *CCAT2* G allele or T allele, pulled down the proteins that bind *CCAT2*, and analyzed them by mass spectrometry (Yoon et al., 2012). Pathway analysis on the QIAGEN platform identified Cleavage and Polyadenylation of Pre-mRNA among the top pathways associated with the G allele (Figure S3A), with CFIm25, the small (25 kDa) subunit of CFIm encoded by the *NUDT21* gene (Elkon et al., 2013; Yang et al., 2011), as the main protein correlated with the pathway. Notably, in the T allele pull down, both CFIm25 and the larger subunit (68 kDa) of the CFIm complex, CFIm68 (encoded by the *CPSF6* gene), were detected (CFIm68 was not detected in the G allele pull down); however, for CFIm25, the area under the peak had a 1.48 higher fold change in the G allele compared to the T allele (Figure S3B). We screened the *GLS* intron 14 for potential splicing and/or alternative polyadenylation (APA) sites using ASTRA (Alternative Splicing and TRanscription Archives database; <http://dbarchive.biosciencedbc.jp/en/astra/desc.html>) (Nagasaki et al., 2006) and identified a type 2 (skipping exon) poly(A) site (Figure S3C) (Lutz and Moreira, 2011) and multiple conserved binding motifs (UGUA) for CFIm25, consistent with a previous report mapping two poly(A) motifs within the same intron of the *GLS* pre-mRNA (Tian et al., 2007). Considering that CFIm25 and the CFIm heterotrimer complex have been previously linked to alternative splicing (Millevoi et al., 2006; Zhou et al., 2002), we first downregulated *NUDT21* and assessed the protein levels of GAC and KGA. We noticed a significant decrease in GAC protein expression in both cellular models and a clear increase in the KGA protein expression (Figure 3A). We also measured mRNA expression for the two isoforms and observed a significant reduction of the GAC/KGA mRNA ratio with *NUDT21* knockdown (Figure 3B). In order to evaluate whether the switch in isoform expression is a consequence of CFIm25 binding to the UGUA sequences within intron 14 of *GLS* pre-mRNA, we designed antisense synthetic oligonucleotides (ASOs) to block the binding of the 25 kDa subunit to these motifs (Figure 3C). Out of the four tested ASOs, we could identify two that were able to reverse the GAC to KGA protein expression ratio similar to the specific downregulation of *NUDT21* in HCT116 OC1 cells (Figure 3C). This result suggested that binding of CFIm25 to intron 14 is responsible for inducing the preferential expression of GAC. To further confirm the direct interaction of CFIm25 with *GLS* pre-mRNA and *CCAT2*, we immunoprecipitated the RNA bound to constituting proteins of the CFIm complex, CFIm25 and CFIm68, in HCT116 cells overexpressing either the G or T allele of *CCAT2* and control cells, and measured the differences in RNA enrichment between the distinct pull-down lysates by real-time quantitative PCR (qRT-PCR) (Figures 3D–3F and S3D–S3F). We included two lncRNAs as controls: *NEAT1* was chosen to be a positive control as it has been previously shown to interact with the CFIm complex (Naganuma et al., 2012), and *GAS5* was chosen as negative control due to minimal sequence similarity with *CCAT2* (Figure S3G). When assessing the fold enrichment of *GLS* and *CCAT2*, we detected, respectively, 5.77 and 13.6 times more RNA bound to CFIm25 in the

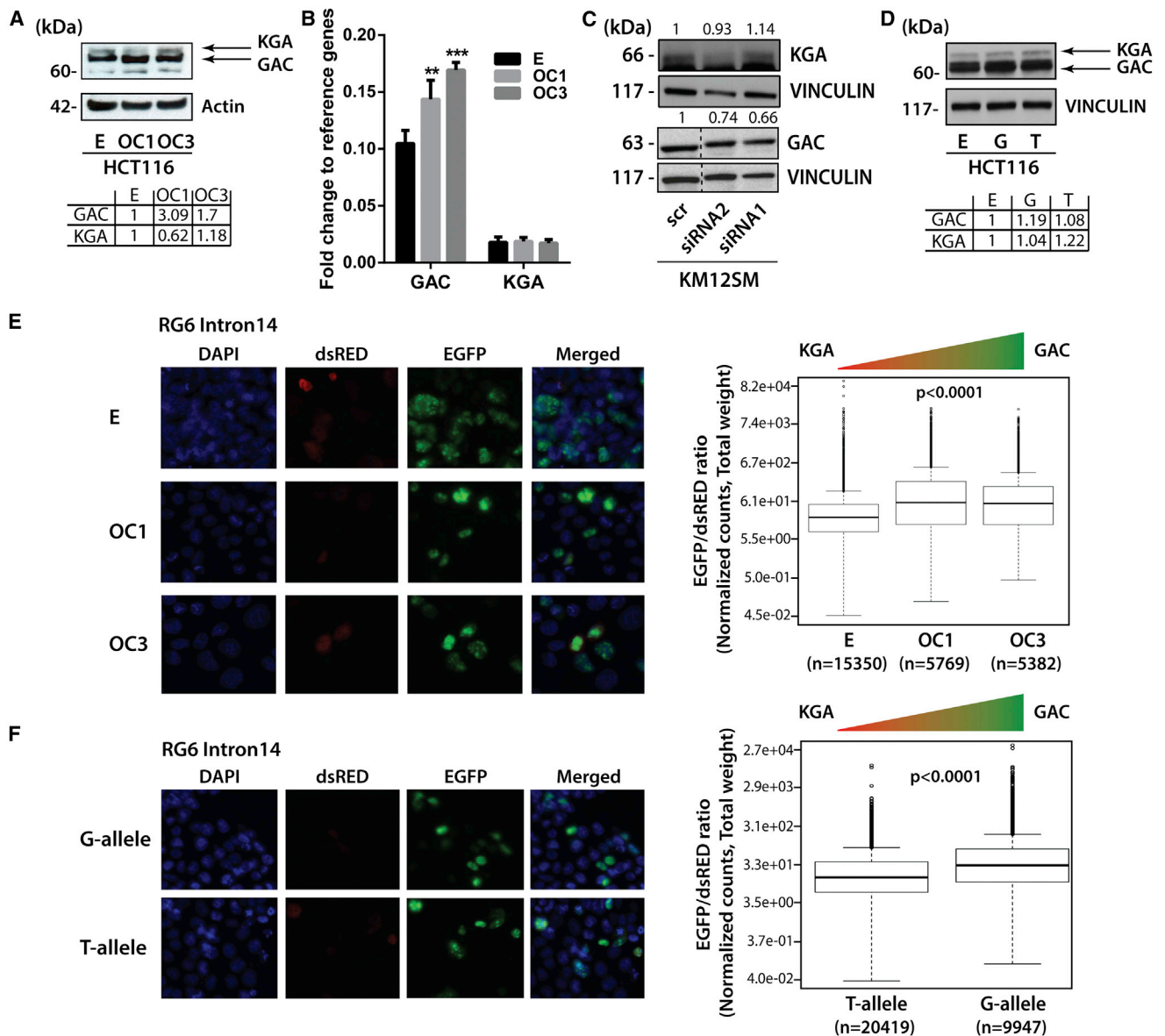


Figure 2. CCAAT2 Induces the Preferential Splicing of GAC

(A) Western blot analysis of GAC, KGA in HCT116 CCAAT2-overexpressing cells (OC1 and OC3) and control cells.

(B) qRT-PCR assessing the mRNA expression of GAC and KGA in HCT116 CCAAT2-overexpressing cells (OC1 and OC3) and control cells.

(C) Western blot analysis of GAC, KGA in KM12SM cells with CCAAT2 downregulation.

(D) Western blot analysis of GAC, KGA in HCT116 stably overexpressing CCAAT2 G or T alleles and control cells.

(E) Fluorescence microscopy images of HCT116 stable clones (E, empty control vector; OC1 and OC3, CCAAT2 overexpressing) transfected with the RG6 intron 14 vector and the analysis of the EGFP/dsRED ratio (n = number of analyzed cells).

(F) Fluorescence microscopy images of HCT116 CCAAT2 G allele and T allele transfected with the RG6 intron 14 vector and the analysis of the EGFP/dsRED ratio (n = number of analyzed cells).

Results are presented as normalized mean values \pm SD. See also Figure S2 and Table S2.

cells overexpressing CCAAT2 G allele compared to control cells, while in the cells overexpressing CCAAT2 T allele compared to control cells, the fold enrichment ratios were only about half (2.95 and 6.02, respectively) (Figure 3D). Moreover, comparing the fold enrichment in the G-overexpressing cells to the T-overexpressing cells, we observed roughly double fold enrichment in

the G-overexpressing cells for both GLS and CCAAT2 (1.95 and 2.26) (Figures 3E and 3F). The positive control (NEAT1) presented 6.3-fold more RNA bound to CFIm25 in the cells overexpressing CCAAT2 G allele compared to control cells and 2.79-fold more RNA enrichment in the cells overexpressing CCAAT2 T allele compared to control cells (Figures 3D and S3D). The negative

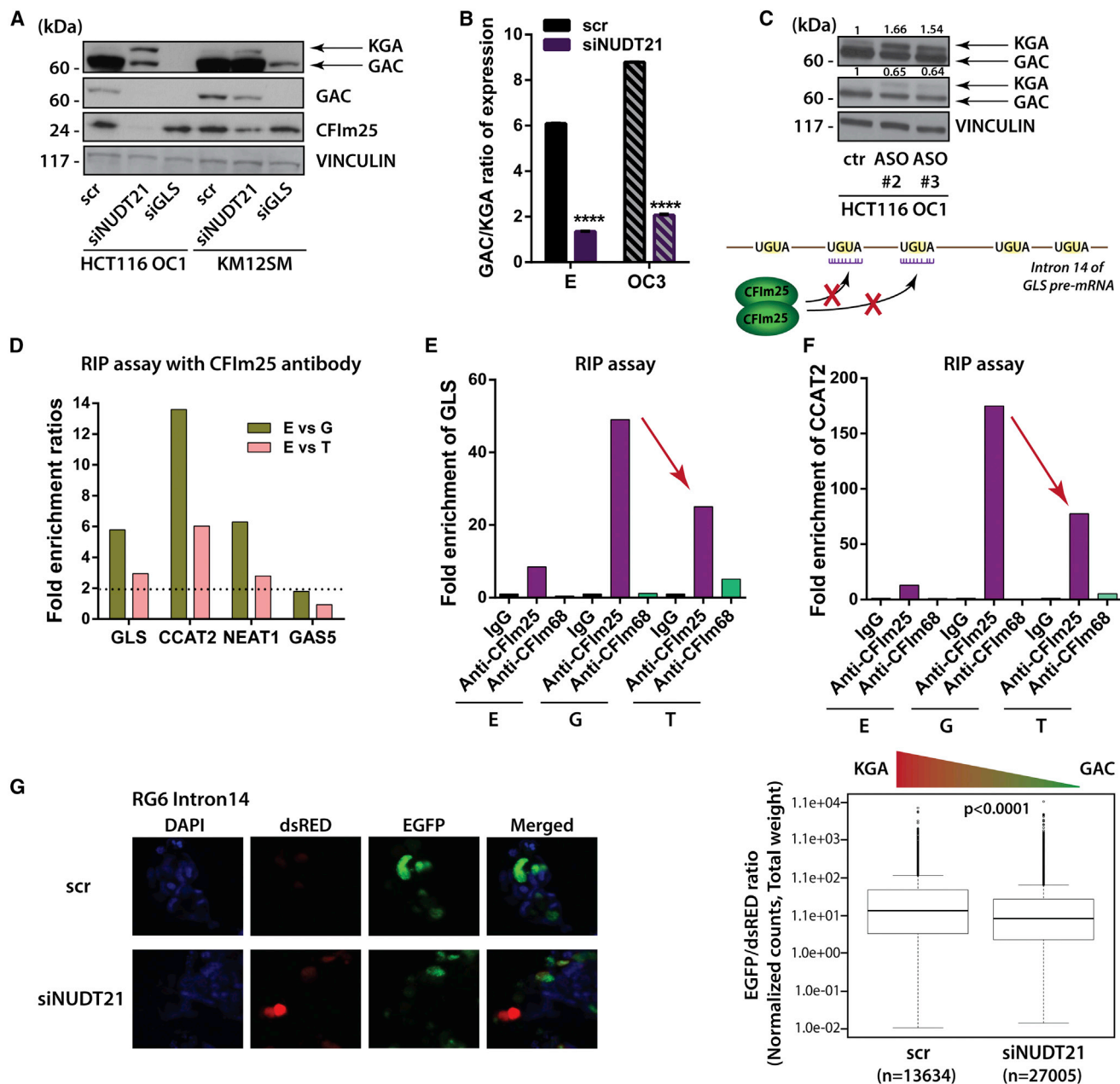


Figure 3. CFIm Protein Complex Binds *GLS* Pre-mRNA

(A) Western blot analysis of CFIm25, GAC, and KGA in HCT116 OC1 and KM12SM cells transiently transfected with siRNA for NUDT21, GLS (targeting the coding sequence shared by the two isoforms), and siRNA control.

(B) qRT-PCR assessing the GAC/KGA mRNA ratio in HCT116 *CCAT2*-overexpressing cells (OC1 and OC3) and control cells (E) with modulated CFIm25 expression.

(C) Western blot analysis of GAC and KGA in HCT116 OC1 cells with transient blockage of CFIm25 binding motifs (UGUA) by antisense oligonucleotides (ASOs). Schematic representation of the mechanism is presented below.

(D) qRT-PCR assessing the fold enrichment of *GLS*, *CCAT2*, *NEAT1*, and *GAS5* RNA bound to CFIm25 protein (RNA immunoprecipitation). Data are presented as fold enrichment ratios between control HCT116 cells (E) and *CCAT2*-overexpressing G or T allele.

(E and F) qRT-PCR assessing the fold enrichment of *GLS* mRNA (E) and *CCAT2* (F) bound to CFIm25 and CFIm68 in HCT116 cells, *CCAT2*-overexpressing G or T alleles, and control cells (E).

(G) Fluorescence microscopy images of KM12SM cells transfected with siNUDT21 and scr, followed by transfection with the RG6 intron 14 vector, and the analysis of the EGFP/dsRED ratio (n = number of analyzed cells).

Results are presented as normalized mean values \pm SD. See also Figure S3 and Table S2.

control (*GAS5*) revealed only a 1.79-fold increase in the RNA bound to CFIm25 in the cells overexpressing *CCAT2* G allele compared to control cells and no difference in RNA enrichment between the overexpressing *CCAT2* T allele and control cells (Figures 3D and S3E). Thus, we concluded that, overall, in the cells overexpressing *CCAT2*, there is an augmentation of interaction between CFIm25 and *GLS* and *CCAT2*, with the highest levels in the G-overexpressing cells. The low binding of the RNAs to the CFIm68 was not surprising, as the main function of the protein is merely to enhance RNA binding and facilitate RNA looping, while the 25 kDa subunit has the leading role in binding the RNA via the UGUA elements (Yang et al., 2011) (Figures 3E, 3F, S3D, and S3E). Nonetheless, for our RNAs of interest, we observed an increase in enrichment in the T allele overexpressing cells compared to the G allele overexpressing and control cells, suggesting the secondary structure of *CCAT2* T allele may ease the interaction between the 68 kDa subunit and RNA molecules. In addition, we confirmed these results by end-point PCR in both the same cellular model and the KM12SM cell line, with a GT-heterozygous genotype (Figures S4A and S4B). As a further validation, we expressed the RG6 bichromatic fluorescent reporter with the intron 14 in KM12SM cells with knockdown of *NUDT21*. We assessed, by both VECTRA and FACS, the ratio of EGFP to dsRED and found a significantly lower (28%) EGFP/dsRED ratio in the cells with *NUDT21* downregulation, corresponding to fewer splicing events and consequently lower expression of the GAC equivalent (Figure 3G and Table S2).

Alternative Splicing of *GLS* Is Associated with the Interaction between *CCAT2* and the CFIm Complex

We next aimed to investigate in more detail the mechanism leading to the difference in binding affinity of CFIm25 and CFIm68 to the distinct *CCAT2* alleles. We first scanned the *CCAT2* RNA sequence and identified two CFIm25 binding motifs surrounding the rs6983267, one upstream and the other downstream of the SNP. We performed secondary structure predictions using the RNAfold Webserver (<http://rna.tbi.univie.ac.at/cgi-bin/RNAfold.cgi>) and noticed major local structural changes induced near the putative upstream CFIm25 binding sequence, by the single nucleotide variation, especially among the G and T alleles (Figure S4C). Such changes may plausibly translate into distinct tertiary folds that could in principle explain the binding of the G and T alleles with different affinities. To further validate our results and evaluate the contribution of a single nucleotide to the structural changes and binding affinity, we mutated the SNP into an A or C (nucleotides never detected in the human population) and also deleted the 7 nucleotide region encompassing the SNP, which has been reported to have enhancer activity (Tuupainen et al., 2009). We repeated the RNA pull-down assay using different vectors containing the MS2 tags (*CCAT2*-G, -T, -A, -C, and DEL) and analyzed by western blot the proteins bound to RNAs. When CFIm25 antibody was hybridized on the blot, we detected a strong band of approximately 64 kDa unique to the G allele (band corresponds to the CFIm25 dimer; Figure 4A). When CFIm68 antibody was hybridized on the blot, we distinguished bands of approximately 68 kDa for both the T allele and the allele with the deleted region

(Figure 4A). This implied that the T allele preferentially binds the 68 kDa subunit, but not in the region of the SNP. Notably, neither of the two mutated *CCAT2* alleles (A and C) interacted with the CFIm complex, and interestingly, both present secondary structures different from the G and T alleles (Figure S4C).

Additional evidence for the direct interaction between the *CCAT2* G and T alleles with the CFIm complex was provided by a His₆-tag pull-down assay using heterologously expressed CFIm68:CFIm25 complex (His₆-tagged CFIm68 subunit; Figure 4B) incubated with in vitro synthesized RNAs. We detected strong affinity of the CFIm complex for the *CCAT2* G allele, followed by moderate binding of the *CCAT2* T allele. We also identified in the pull down the 600 nt long region of the *GLS* pre-mRNA intron 14, containing one type 2 poly(A) site, with affinities for the protein complex corresponding to the two alleles (Figure 4B). This suggested that the intron 14 may also interact with *CCAT2*. To test this, we added a biotin tag to in vitro transcribed *CCAT2* RNAs, combined them with the intron 14 fragment and/or CFIm complex, and pulled down the complex with Streptavidin beads. We confirmed not only that the *CCAT2* G allele preferentially binds CFIm25, but also that *CCAT2* interacts with the intron 14 fragment in a SNP-independent fashion (Figures 4C and S4D). To ensure the specificity of the interaction, we repeated the biotin RNA pull-down assay to include the biotinylated *CCAT2* C allele as a negative control. We also added the whole intron 14, previously used for the RG6 splicing assay, to determine if *CCAT2* can interact with the entire region. We prepared mixes of *CCAT2* (G, T, and C) and the CFIm complex with and without the intron 14 fragment to evaluate how it impacts the interaction between *CCAT2* and CFIm complex. We discovered that in the presence of the intron 14, *CCAT2* G and T alleles displayed increased binding affinity to the CFIm complex, compared to the C allele (Figures 4D and S4E and Table S3). The G and T alleles presented a remarkable specificity for the CFIm25 dimer in the presence of the intron 14 (both the smaller fragment and the whole intron) with enhanced binding to the G allele (Figure S4E and Table S3), supporting the hypothesis that the secondary structure of *CCAT2* influences the interaction with the protein complex. In the absence of the intron, although the specificity of the interaction with the CFIm25 dimer is partly retained, it appeared to be revoked in the case of CFIm complex (Figures 4D and S4E and Table S3). We confirmed that *CCAT2* G and T alleles can bind the whole intron 14 as well and aligned the *CCAT2* genomic sequence with *GLS* genomic sequence to determine the extent of the interaction (Figure S4F). We observed multiple short fragments (13–18 nt) of sequence complementarity spanning the entire *GLS* sequence, present in both introns and exons (Figure S5A). For additional validation, we performed the His₆-tag pull-down assay using the G, T, and C alleles in the presence and absence of the whole intron 14. As expected, when the intron was included in the mix, we could detect only *CCAT2* G and T alleles in the pull-down lysates (Figure S4G).

Furthermore, the same mixes of *CCAT2* RNA (G/T), CFIm protein complex, and intron 14 RNA were prepared, as well as solutions of individual components, and subjected to atomic force microscopy (AFM) for visualizing the formation of the RNA:protein:RNA quaternary complex (Lyubchenko et al., 2011) (Figures

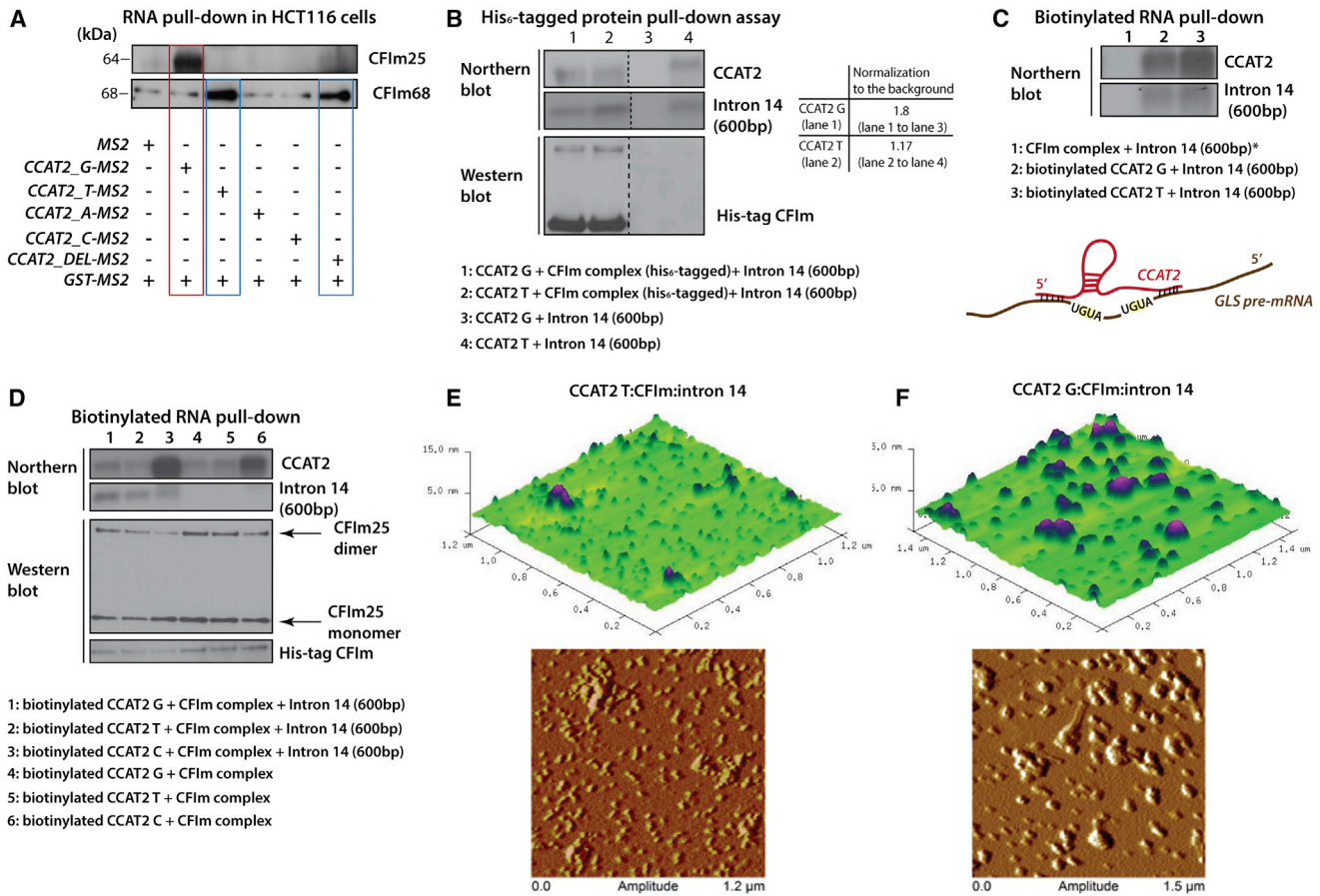


Figure 4. The rs6983267 SNP Affects the Interaction of CCAT2 with the CFIm Protein Complex

(A) Western blot analysis of the proteins pulled down with the MS2-CCAT2 vectors (G, T, A, C, and DEL) showing the presence of CFIm25 for the G allele and CFIm68 for the T allele.

(B) Northern blot analysis showing the presence of CCAT2 and intron 14 (600 bp fragment) in the lysate pulled down with TALON resin (upper panel). Western blot analysis showing the presence of the His₆-tagged CFIm complex in the lysate pulled down with the TALON resin (lower panel).

(C) Northern blot analysis showing the presence of CCAT2 and intron 14 (600 bp fragment) in the lysate pulled down with Streptavidin beads. Lane 1 marked with the star symbol is identical to lane 3 in Figure S4D. Schematic illustration of the interaction of CCAT2 with GLS pre-mRNA (representation is not at scale).

(D) Northern blot analysis showing the presence of CCAT2 and intron 14 (600 bp fragment) in the lysate pulled down with Streptavidin beads (upper panel). Western blot analysis showing the presence CFIm25, monomer (26 kDa) and dimer (64 kDa), and His₆-tagged CFIm68 (38 kDa) (lower panel).

(E and F) AFM images of CCAT2:CFIm:intron 14 quaternary complex including either CCAT2 T allele (E) or CCAT2 G allele (F).

See also Figures S4 and S5 and Table S3.

4E and 4F). Particles of substantial size were detected when scanning the mica surface, suggesting the formation of potential CCAT2:CFIm:intron14 complexes, with higher frequency for the G allele compared to the T allele (Figures 4E and 4F), while the individual components (CFIm protein complex, CCAT2 RNA, and intron 14 RNA) appeared to be evidently smaller (Figures S5B–S5D). Moreover, when measuring the diameter of the complexes (G allele complex, 226.706 nm; T allele complex, 182.844 nm), we found that it corresponds approximately to the sum of the diameter of individual components (CCAT2, 81.865 nm; CFIm, 67.999 nm; intron 14, 48.360 nm).

Collectively, these findings suggested that: (1) GLS pre-mRNA impacts the interaction of CCAT2 with CFIm complex; (2) CCAT2 may be acting as a scaffold or assembly platform, promoting the selection of the poly(A) site in intron 14 of GLS pre-mRNA by

directly binding both the pre-mRNA and the CFIm complex; and (3) the formation of the RNA:RNA:protein complex is dependent on the rs6983267 SNP and the secondary structure of CCAT2.

As an additional layer of regulation, we discovered that MYC is a transcription factor for *NUDT21* (data available from authors upon request).

GAC Promotes Metastases and Cell Proliferation

We proceeded with evaluating the contribution of GAC to aggressiveness of CRC. Considering that we have previously demonstrated that CCAT2 promotes metastases (Ling et al., 2013b), we first assessed the in vitro migration potential of HCT116 CCAT2-overexpressing cells treated with either the allosteric inhibitor 968 or siRNA for GLS (Katt et al., 2012). We

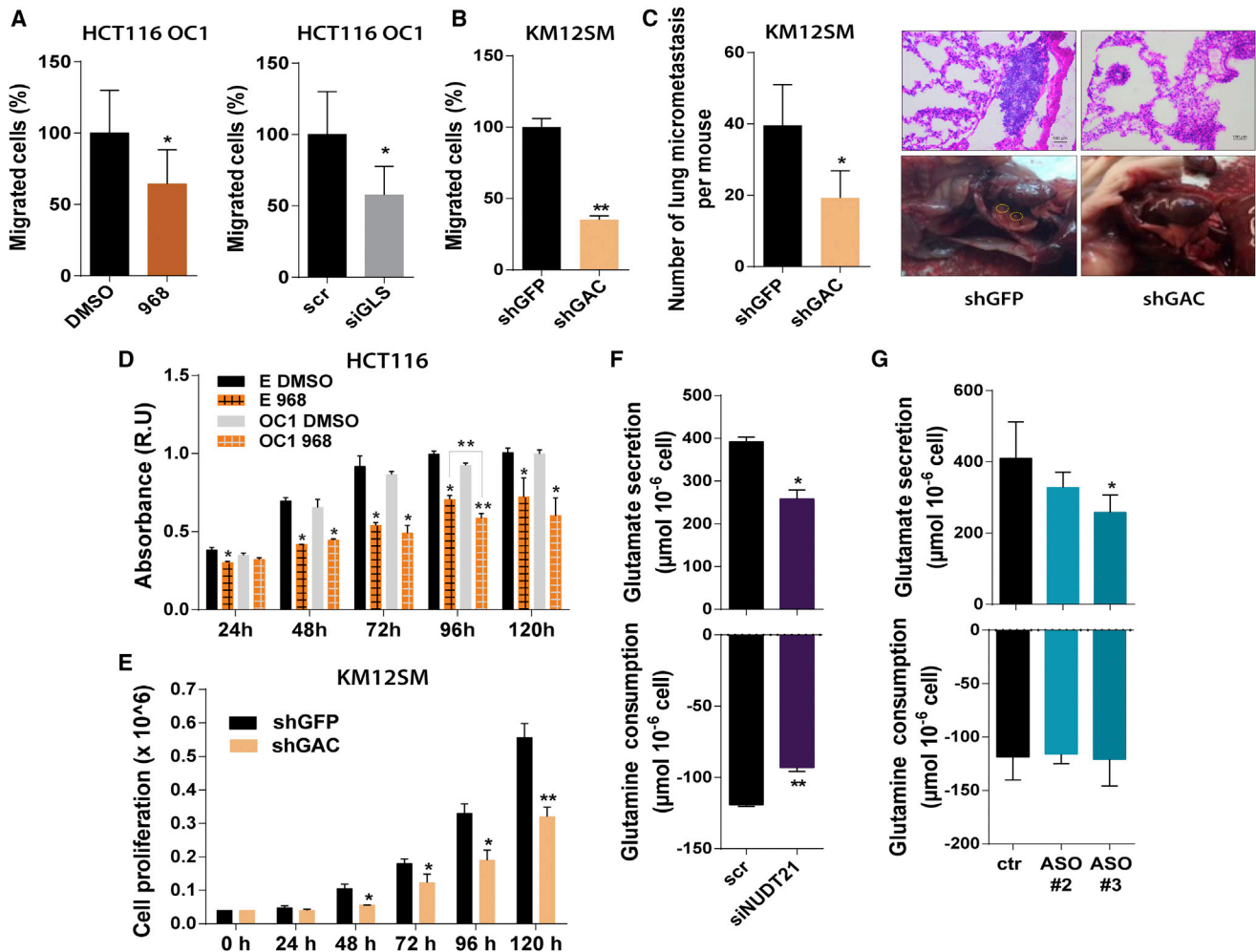


Figure 5. GLS Promotes In Vivo Metastases and In Vitro Cell Proliferation and Migration

(A) Migration of HCT116 OC1 cells (GG genotype) treated with the inhibitor 968 and DMSO (left panel) and with siGLS and scrambled siRNA (right panel). (B) Migration of KM12SM cells (GT genotype) with stable downregulation of GAC. KM12SM shGFP cells represent the control cells. (C) Number of the lung micrometastases for two groups (shGFP, 4 mice; shGAC, 4 mice) assessed by IHC (left panel). IHC images showing micrometastases in the three groups and images showing the presence or absence of lung metastases for mice injected in the tail vein with KM12SM shGFP and shGAC cells, respectively (right panel). (D and E) Growth curves for HCT116 OC1 and control cells (GG genotype) treated with DMSO (control) or the GLS allosteric inhibitor 968 (10 μ M) (D) and KM12SM cells (GT genotype) with stable downregulation of GAC (E). (F and G) Glutamine and glutamate concentration in the media relative to the empty well 24 hr after seeding HCT116 CCAT2-overexpressing cells (OC1, GG genotype) transfected with siRNA against *NUDT21* and scrambled (F) and ASOs for inhibiting the binding sites of CFIm25 (G). Results are presented as normalized mean values \pm SD. See also Figure S6 and Table S4.

observed a reduction by half of the migration in the cells where GLS was either inhibited or downregulated (Figure 5A). We next assessed the individual contribution of GAC to the migration, in KM12SM cells with stable downregulation of the isoform (Figure S6A), and found that 60% fewer cells migrated when GAC expression was reduced (Figure 5B). We then injected the KM12SM stable clones in the tail vein of nude mice, sacrificed the mice 8 weeks after injections, and evaluated the in-lung macro- and micrometastases. Supporting our in vitro results, the incidence of metastases to the lung was 50% higher in the mice injected with the control cells (shGFP) compared to the shGAC group (Figure 5C). Moreover, when

we assessed the proliferation of HCT116 control and CCAT2-overexpressing cells treated with the GLS inhibitor 968, we found that cells overexpressing CCAT2 were more sensitive to GLS (GAC in this case) inhibition, implying that cells with high CCAT2 expression are dependent on GAC for survival (Figure 5D) (Katt et al., 2012; Wang et al., 2010a). Similar results were obtained when using KM12SM cells with GAC downregulation compared to control cells in vitro (Figure 5E). Additional confirmation of the higher dependency of the CCAT2 G allele on GAC was provided by the colony formation assay for NIH 3T3 cells transfected with the CCAT2-overexpressing vectors (Figures S6B and S6C).

We next sought to determine if the shift in *GLS* isoform expression and CFIm25 is responsible for the marked metabolic changes observed in cells overexpressing *CCAT2*. We therefore modulated the expression of the isoforms using the ASOs and downregulated *NUDT21* in HCT116 *CCAT2*-overexpressing cell line (OC1) and measured the extracellular lactate concentration and glutamine metabolism. We observed that downregulation of *NUDT21* significantly decreased lactate and glutamate secretion and glutamine consumption similarly to the effects of *CCAT2* overexpression in the same cell line (Figures S6D and 5F). However, these metabolic changes appeared to only partly mirror the metabolic effects of *CCAT2* overexpression, suggesting there are additional layers of regulations independent of *NUDT21*, most likely through the bona fide cancer metabolism modulator and *CCAT2* target, *MYC*. On the other hand, the switch in *GLS* isoforms reflected in lower secretion of glutamate with the glutamine consumption remaining relatively constant but had a modest effect on the extracellular levels of lactate (Figures 5G and S6E). These findings suggested that *GLS* is not the only contributor to *CCAT2*-induced metabolic profile. We hypothesized that other metabolic targets might be regulated by *CCAT2* via the same mechanism; thus, we performed Affymetrix HTA 2.0 array to compare the whole transcriptome splicing pattern in HCT116 *CCAT2*-overexpressing G and T allele cells. Pathway analysis revealed that several genes associated with two major metabolic pathways, “Metabolism of Carbohydrates” and “Fructose and Mannose Metabolism,” are significantly spliced between the *CCAT2* G and T alleles (Table S4). Moreover, validating our previous results, we identified a negative splicing index (SI = -1.19) for *GLS* for the exclusion junction connecting exon 14 and exon 15, suggesting higher signal for the exclusion junction in the T allele-expressing cells. This translates into less GAC being spliced in the T allele cells compared to the G allele cells, supportive of our findings (Figure S6F).

Collectively, these data demonstrate that GAC adds to the CRC phenotype; however, it is not solely responsible for the metabolic phenotype observed in cells overexpressing *CCAT2*.

CCAT2-CFIm-GLS Regulation Axis in CRC Tumors

We continued with evaluating the expression pattern of *CCAT2*, *GLS*, *NUDT21*, and *CPSF6* in colon tumors by analyzing the publicly available TCGA database of colon cancer (<http://cancergenome.nih.gov/>). We first compared 18 normal samples to 193 tumor samples and identified an enrichment of the GAC isoform, as well as *NUDT21* and *CPSF6* in tumor tissue, whereas *KGA* showed the opposite pattern (Figures 6A–6D). We further analyzed the associations between *CCAT2*, *NUDT21*, *CPSF6*, *GAC*, and *KGA* in the TCGA dataset of colon cancer samples (Cancer Genome Atlas Network, 2012) and detected direct correlations of *CCAT2*, *CPSF6*, and *NUDT21* with *GAC* ($r_s = 0.26$, $p = 0.0006$; $r_s = 0.68$, $p < 0.0001$; and $r_s = 0.72$, $p < 0.0001$, respectively; Figure S7A) and inverse correlations between *CCAT2*, *CPSF6*, *NUDT21*, and *KGA* ($r_s = -0.17$, $p = 0.0271$; $r_s = -0.47$, $p < 0.0001$; and $r_s = -0.60$, $p < 0.0001$; Figure S7A), as well as between *KGA* and *GAC* ($r_s = -0.590$, $p < 0.0001$) (Figure S7A). We also obtained significant direct associations of *CCAT2* with *CPSF6* and *NUDT21* ($r_s = 0.20$, $p = 0.0082$ and $r_s = 0.26$, $p =$

0.0007; Figure S7A). We did not find any significant correlations between the expression of *MYC* and *NUDT21*, *GAC*, or *KGA*. Since our in vitro findings advanced the concept that *CCAT2* G allele is promoting the expression of *GAC*, we compared the levels of *GAC* and *KGA* between patients having GG, GT, and TT genotypes. We observed a significant association with the genotypes for *GAC*, having the highest expression in patients with GG genotype, but not for *KGA* (Figures 6E and S7B). Similarly, we did not find any association of *NUDT21* or *MYC* with the genotypes (Figures S7C and S7D). These results suggested the molecular mechanism uncovered in vitro is present in CRC patients. Moreover, we analyzed the correlation between the expression of the two isoforms and the overall survival of patients from the TCGA dataset and observed a significant association of high *GAC* expression combined with low *KGA* expression with shorter overall survival (Figure S7E). This suggested that the *GAC* isoform may accelerate the progression of cancer. In addition, we interrogated the TCGA colon cancer dataset for genes that significantly correlate with the lncRNA and performed gene set enrichment analysis (GSEA) and ingenuity pathway analysis (IPA) (QIAGEN) to identify the *CCAT2* gene signatures. Various metabolically relevant pathways were found significantly associated with *CCAT2* expression by both analyses (Figures 7A and 7B). We further inquired as to whether the genes that were found significantly correlated with *CCAT2* expression were also associated with the genotypes of rs6983267 SNP. We repeated the GSEA and screened for pathways that correlated with either of the genotypes (FDR q value < 0.25 and nominal p value < 0.05). We identified various metabolic and RNA processing pathways that were associated with certain genotypes (Figure 7C). Interestingly, several of the pathways were related to the ones identified by the Affymetrix HTA 2.0 array (highlighted in green in Figure 7C), suggesting that *CCAT2* may modulate cellular metabolism in CRC patients through a network of metabolic genes regulated most likely via the same mechanism of alternative splicing (see Table S4).

To assess the protein expression of CFIm68, CFIm25, *GAC*, and *KGA*, we performed western blot analysis on paired normal mucosae and CRC samples (patient cohort #1) and identified the same high protein levels of CFIm25 and *GAC* in tumor tissue compared to normal mucosae for 61.5% (8/13) of the pairs (Figure 6F). As for the *KGA* isoform, protein levels were mostly lower in tumor samples or comparable to the levels in normal samples (Figure 6F). The 68 kDa subunit of the CFIm complex was either very low or not expressed in approximately half of the paired samples (7/13), while in the rest of the pairs it was clearly overexpressed in tumors (Figure S7F). We also measured *CCAT2* expression by qRT-PCR in the same set of samples and confirmed a positive correlation between *CCAT2*, CFIm25, and *GAC* for 69.2% of the samples (Figures 6F, 6G, S7G, and S7H). Moreover, the samples that had elevated levels of *CCAT2* displayed a high *GAC/KGA* ratio ($GAC/KGA = 2-5.7$) (Figure S7I). We repeated the measurements in a second set of paired normal mucosae and CRC samples (patient cohort #2) and obtained similar results (Figures S7J and S7K). Both CFIm25 and *GAC* proteins were overexpressed in 60% (3/5) of tumor samples. In all samples, elevated protein levels of CFIm25 and *GAC* matched the increased RNA levels of

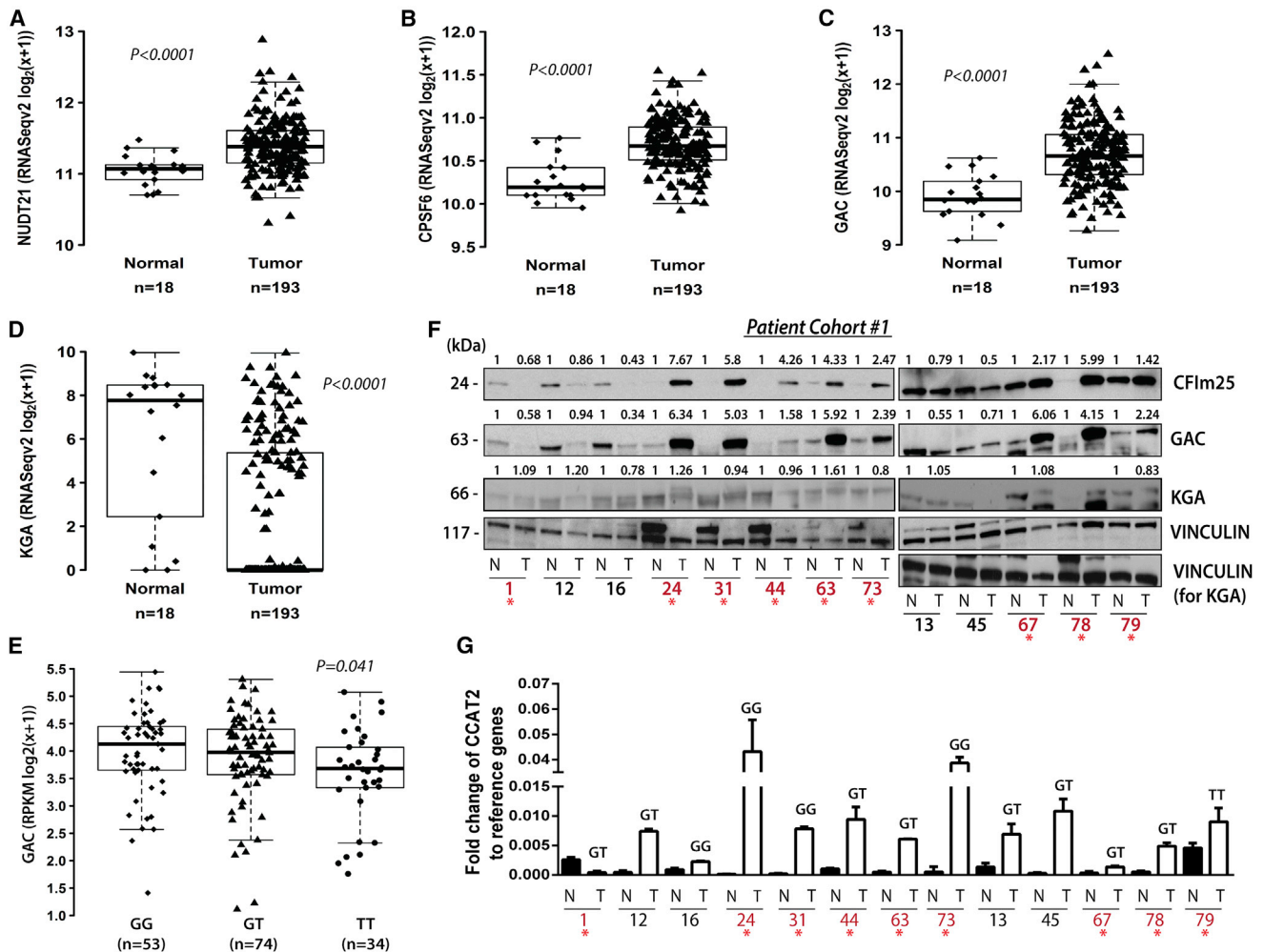


Figure 6. *CCAT2*, *NUDT21*, *CPSF6*, and *GAC* Expression Pattern in TCGA Dataset and CRC Patient Samples

(A–D) Analysis of *NUDT21* (A), *CPSF6* (B), *GAC* (C), and *KGA* (D) mRNA expression in TCGA RNA-seq colon cancer sample set.

(E) Association of *GAC* mRNA expression with the genotypes (GG, GT, and TT) of the rs6983267 SNP for CRC patients (TCGA RNA-seq dataset).

(F) Western blot analysis of CFIm25, *GAC*, and *KGA* expression in paired CRC samples (patient cohort #1).

(G) qRT-PCR analysis for *CCAT2* in the same paired CRC samples (patient cohort #1).

Results are presented as normalized mean values \pm SD. See also Figure S7.

CCAT2. Additionally, we have genotyped the tumors from patient cohort #1 and found that the association of GG genotype with higher *GAC* and CFIm25 protein expression (samples marked in red) was consistent for 75% of patients (3/4), while for the GT genotype the association was present in only 62.5% of patients (5/8) (Figure 6G). No conclusion can be drawn for the TT genotype due to the limited representation of the genotype in this cohort (one patient). Altogether, this mechanism of *GLS* regulation was detected in the majority of the analyzed CRC cases (61%, 11/18).

DISCUSSION

Our study demonstrates that the rs6983267 SNP (G/T) induces changes in the secondary structure of the lncRNA, *CCAT2*, initiating a domino effect mechanism, which leads to allele-specific

reprogramming of cellular energy metabolism. The consequence of the allele-specific interaction between *CCAT2*, CFIm, and *GLS* pre-mRNA appears to be the selection of the poly(A) site within intron 14 of *GLS*, resulting in the preferential splicing to the *GAC* isoform, the more catalytically active of the two *GLS* isoforms (Cassago et al., 2012). Although a recent study has described the negative regulation of *GLS* by CFIm25 in glioblastoma via 3' UTR processing mechanisms (Masamha et al., 2014), suggesting a tumor-suppressive role for CFIm25, in our model, neither of the *GLS* isoforms is subjected to 3' UTR shortening (data not shown). In the context of these findings and considering that *CCAT2* is not expressed in glioblastoma (data not shown), our results reveal an intriguing aspect of lncRNA mechanism of action, namely the ability of an lncRNA to alter the function of the partner RNA-binding protein/complex. The enrichment on metabolites related to TCA cycle that we

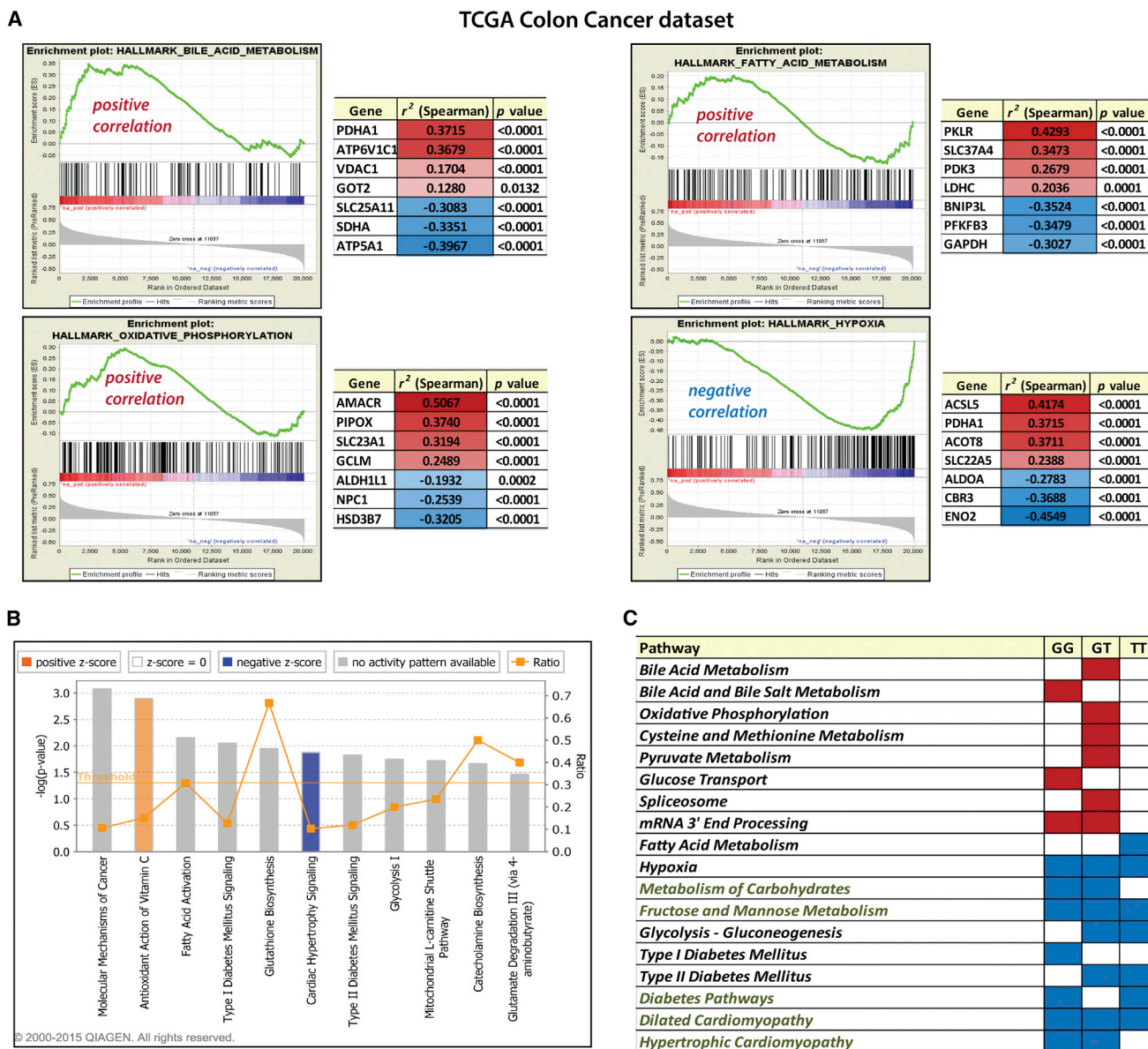


Figure 7. CCAT2 Gene Signature in Colon Cancer Patients – TCGA Dataset

(A and B) Genes associated with CCAT2 were analyzed by gene set enrichment analysis (GSEA) (A) and ingenuity pathway analysis (IPA, QIAGEN) (B). Relevant examples for each analysis are presented in (A) and (B).

(C) Table containing the pathways significantly associated with CCAT2 expression and rs6983267 genotype (FDR q value < 0.25 and nominal p value < 0.05). Pathways that were positively correlated are marked with red, and the ones that are negatively correlated are marked with blue. Highlighted in green are the pathways found common between GSEA analysis and the Affymetrix HTA 2.0 pathways analysis.

See also Figure S7 and Table S4.

observed for tumors derived from HCT116 cells overexpressing CCAT2 the G allele are supported by Kaldma and colleagues' findings describing that CRC tumors are not purely glycolytic, but rather dependent on OXPHOS for ATP production (Kaldma et al., 2014).

The aberrant expression of GLS has been reported in many types of cancer, including CRC (Huang et al., 2014) Furthermore, various studies have described GAC as the more abundant isoform in lung adenocarcinoma, head and neck squamous

cell carcinoma, kidney renal clear cell carcinoma, and AML (Jacque et al., 2015; van den Heuvel et al., 2012; Xia et al., 2014). Glutamine metabolism has also been associated with genomic instability (Jeong et al., 2013), commonly encountered in CRC and previously shown to be promoted by CCAT2 (Ling et al., 2013b), and appears to be endorsed by the G risk allele. However, it must be stated that CCAT2 is modulating energy metabolism in a general fashion via MYC and in an allele-specific manner via GLS and other metabolic enzymes and/or

metabolites, whose expression is finely regulated by the interaction of *CCAT2* with CFIm. Although the differences in regulation between the G and T alleles may not be impressive, the variation in expression of multiple enzymes/metabolites may have an additive effect towards a clear phenotypical change. The complex mechanism presented in this manuscript encompassing lncRNA, protein complexes, oncogenes, and transcription factors opens several windows for targeted therapy. The metabolic enzyme *GLS* is already considered a therapeutic target for cancer (Vander Heiden, 2011); however, our work introduces the opportunity of targeting the cancer-specific GAC isoform in particular.

Lastly, our study reveals the complexity and refinement of the interaction networks among the alleles of a non-coding RNA, the components of a protein complex, and the splicing isoforms of a metabolic enzyme that contribute to the malignant transformation and progression of CRC.

EXPERIMENTAL PROCEDURES

Full details of the [Experimental Procedures](#) are presented in the [Supplemental Experimental Procedures](#). Primer sequences and information regarding the antibodies used in this study can be found in [Tables S5](#) and [S6](#).

Patient Samples

18 paired samples, normal colon mucosa and colon tumor, were used in this study. The samples were obtained from two different sources: The Ruder Boskovic Institute, Croatia (15 paired samples) and University of Ferrara, Italy (5 paired samples). Tissue samples were obtained from fresh surgical specimens frozen in liquid nitrogen and stored at -80°C . All the samples were obtained with the patients' informed consent and under the approval and supervision of the institutional review boards. The samples were histologically confirmed prior to use.

In Vivo Models and Tissue Processing

70 male athymic nude mice were purchased from the National Cancer Institute, Frederick Cancer Research and Development Center (Frederick, MD) and were cared for according to guidelines set forth by the American Association for Accreditation of Laboratory Animal Care and the U.S. Public Health Service policy on Human Care and Use of Laboratory Animals. All mouse studies were approved and supervised by the MD Anderson Cancer Center Institutional Animal Care and Use Committee.

Glucose Uptake Assay

Cells were plated in 96-well plates (25,000 cells/well) 16 hr before performing the assay. The medium was removed and cells were washed twice with PBS. To the wells containing the blanks, 50 μl of PBS was added, while for the wells with the samples 50 μl of 2-NBDG (100 μM) (Sigma) was added and the mixture was incubated for 10 min at 37°C and 5% CO_2 . After incubation, cells were washed twice with ice-cold PBS to stop the reaction, and 200 μl PBS was added to each well. Fluorescence measurements were performed at 485/520 nm with the PHERAstar FS (BMG Labtech).

Lactate Production Assay

To measure lactate production, cells that were 80% confluent were replenished with fresh medium. Aliquots of the medium were removed at the indicated time points (24 or 48 hr) for measurement of lactate using an Accutrend lactate analyzer (Roche). At each time point, cell numbers were also counted for normalization of lactate generation.

Intracellular Glutamate Assay

The glutamate concentration in cell lysates was measured using the Glutamate Colorimetric Assay Kit (Biovision) following the manufacturer's protocol.

Briefly, 1×10^6 cells per tested sample were homogenized in 100 μl of assay buffer and centrifuged to remove insoluble material. 100 μl of reaction mix was added to the supernatant, standards, and background control samples, and after 30 min incubation at 37°C , absorbance was measured at 450 nm with a SpectraMax Plus384 MicroPlate Reader (Molecular Devices). The experiment was performed in quadruplicate.

SUPPLEMENTAL INFORMATION

Supplemental Information includes Supplemental Experimental Procedures, seven figures, and six tables and can be found with this article online at <http://dx.doi.org/10.1016/j.molcel.2016.01.015>.

AUTHOR CONTRIBUTIONS

Conceived and designed the experiments: R.S.R., L.E.V., W.L., J.F.O., A.F.F., M.S.R., M.I., G.B., M.F.F., S.H., W.R.W., A.L.B.A., S.M.G.D., and G.A.C. Performed the experiments: R.S.R., L.E.V., W.L., J.F.O., C.R.-A., D.A., B.P., A.T., Y.C., K.V.R., S.C., M.S., Y.A., L.H.C., G.Y.H., P.M., M.S.R., T.C.I., L.V., and H.L. Analyzed the data: R.S.R., L.E.V., W.L., J.F.O., C.I., C.R.-A., D.A., A.T., A.F.F., L.V., G.K., J.A.B., M.R., A.L.B.A., S.M.G.D., and G.A.C. Contributed reagents/materials/analysis tools: L.H., S.K., R.G., G.L., S.Y.L., R.C.B., P.H., M.G.R., I.B.-N., and G.L.-B. Wrote the first draft of the manuscript: R.S.R., S.M.G.D., A.L.B.A., and G.A.C. Contributed to the writing of the manuscript: R.S.R., S.M.G.D., A.L.B.A., and G.A.C. Agree with manuscript results and conclusions: all authors. Critical revision of the manuscript for important intellectual content: all authors. Statistical analysis: C.I., L.H., G.K., M.R., and H.L. Study supervision: S.M.G.D. and G.A.C.

ACKNOWLEDGMENTS

G.A.C. is The Alan M. Gewirtz Leukemia & Lymphoma Society Scholar. Work in G.A.C.'s laboratory is supported in part by the NIH/NCI grants 1UH2TR00943-01 and 1 R01 CA182905-01, the UT MD Anderson Cancer Center SPORE in Melanoma grant from NCI (P50 CA093459), Aim at Melanoma Foundation and the Miriam and Jim Mulva research funds, the Brain SPORE (2P50CA127001), the Center for Radiation Oncology Research Project, the Center for Cancer Epigenetics Pilot project, a 2014 Knowledge GAP MDACC grant, a CLL Moonshot pilot project, the UT MD Anderson Cancer Center Dun-can Family Institute for Cancer Prevention and Risk Assessment, a SINF grant in colon cancer, the Laura and John Arnold Foundation, the RGK Foundation, and the Estate of C.G. Johnson, Jr. I.B.-N. was financed by a grant entitled Non-Invasive Intelligent Systems for Colorectal Cancer Diagnosis and Prognosis Based on circulating miRNAs Integrated in the Clinical Workflow – INTEL COR. S.M.G.D., A.L.B.A., and D.A. are supported by the São Paulo Research Foundation FAPESP under grants 2014/15968-3, 2014/20673-2, and 2014/17820-3, respectively. W.L. was partly supported by grants from The University of Texas MD Anderson Cancer Center Sheikh Ahmed Bin Zayed Al Nahyan Center for Pancreatic Cancer Research. J.A.B. was supported by the Cancer Center Support Grant (P30 CA016672), and the HP imaging program of the Small Animal Facility (SAIF) was supported by the Cancer Prevention and Research Institutes of Texas grant RP-101243P5. H.L. was supported by NIH/NCI grant R01CA175486, a grant (RP140462) from the Cancer Prevention and Research Institute of Texas, and the R. Lee Clark Fellow Award from The Jeanne F. Shelby Scholarship Fund. I.B.-N. was financed by a Fulbright fellowship and by a grant entitled Non-Invasive Intelligent Systems for Colorectal Cancer Diagnosis and Prognosis Based on circulating miRNAs Integrated in the Clinical Workflow – INTEL COR. We would like to thank Dr. Riccardo Fodde (Erasmus Medical Center) for the scientific support and advice, Dr. Sylvie Doublet for the generous gift of CFIm25 and CFIm68 plasmids, Dr. Riccardo Spizzo for generating the HCT116 *CCAT2* stable clones, and Dr. Thomas A. Cooper for the generous gift of RG6 plasmid. We would also like to thank the IM Bioscope II-UT core facility and Dr. Ana Maria Zaske for performing the AFM imaging. Additionally, we thank the members of Flow Cytometry & Cellular Imaging Core Facility (Department of Leukemia) and Dr. Jared Burks for performing the VECTRA imaging and analysis and

Drs. Liuqing Yang (MDACC), Yibin Zhou (IBT), Clifford Stephan (IBT), Shawn Bratton (MDACC), Charles V. Kingsley (MDACC), Jorge Delacera (MDACC), Iva Maestri (University of Ferrara), and Linda Ulazzi (University of Ferrara) for the technical support. We also would like to thank the Biological Imaging Facility and the Protein Purification and Bioassay Laboratories (LNBio/CNPEM/Brazil) for access to the equipment.

Received: April 3, 2015

Revised: October 23, 2015

Accepted: January 8, 2016

Published: February 4, 2016

REFERENCES

- Bester, A.C., Roniger, M., Oren, Y.S., Im, M.M., Sarni, D., Chaoat, M., Bensimon, A., Zamir, G., Shewach, D.S., and Kerem, B. (2011). Nucleotide deficiency promotes genomic instability in early stages of cancer development. *Cell* **145**, 435–446.
- Boroughs, L.K., and DeBerardinis, R.J. (2015). Metabolic pathways promoting cancer cell survival and growth. *Nat. Cell Biol.* **17**, 351–359.
- Cancer Genome Atlas Network (2012). Comprehensive molecular characterization of human colon and rectal cancer. *Nature* **487**, 330–337.
- Carroll, P.A., Diolaiti, D., McFerrin, L., Gu, H., Djukovic, D., Du, J., Cheng, P.F., Anderson, S., Ulrich, M., Hurley, J.B., et al. (2015). Deregulated Myc requires MondoA/Mlx for metabolic reprogramming and tumorigenesis. *Cancer Cell* **27**, 271–285.
- Cassago, A., Ferreira, A.P., Ferreira, I.M., Fornezari, C., Gomes, E.R., Greene, K.S., Pereira, H.M., Garratt, R.C., Dias, S.M., and Ambrosio, A.L. (2012). Mitochondrial localization and structure-based phosphate activation mechanism of Glutaminase C with implications for cancer metabolism. *Proc. Natl. Acad. Sci. USA* **109**, 1092–1097.
- Chen, J.Q., and Russo, J. (2012). Dysregulation of glucose transport, glycolysis, TCA cycle and glutaminolysis by oncogenes and tumor suppressors in cancer cells. *Biochim. Biophys. Acta* **1826**, 370–384.
- Elkon, R., Ugalde, A.P., and Agami, R. (2013). Alternative cleavage and polyadenylation: extent, regulation and function. *Nat. Rev. Genet.* **14**, 496–506.
- Gao, P., Tchernyshyov, I., Chang, T.C., Lee, Y.S., Kita, K., Ochi, T., Zeller, K.I., De Marzo, A.M., Van Eyk, J.E., Mendell, J.T., and Dang, C.V. (2009). c-Myc suppression of miR-23a/b enhances mitochondrial glutaminase expression and glutamine metabolism. *Nature* **458**, 762–765.
- Huang, F., Zhang, Q., Ma, H., Lv, Q., and Zhang, T. (2014). Expression of glutaminase is upregulated in colorectal cancer and of clinical significance. *Int. J. Clin. Exp. Pathol.* **7**, 1093–1100.
- Jacque, N., Ronchetti, A.M., Larrue, C., Meunier, G., Birsén, R., Willems, L., Saland, E., Decroocq, J., Thiago, T.T., Lambert, M., et al. (2015). Targeting glutaminolysis has antileukemic activity in acute myeloid leukemia and synergizes with BCL-2 inhibition. *Blood* **126**, 1346–1356.
- Jeong, S.M., Xiao, C., Finley, L.W., Lahusen, T., Souza, A.L., Pierce, K., Li, Y.H., Wang, X., Laurent, G., German, N.J., et al. (2013). SIRT4 has tumor-suppressive activity and regulates the cellular metabolic response to DNA damage by inhibiting mitochondrial glutamine metabolism. *Cancer Cell* **23**, 450–463.
- Kaldma, A., Klepinin, A., Chekulayev, V., Mado, K., Shevchuk, I., Timohina, N., Tepp, K., Kandashvili, M., Varikmaa, M., Koit, A., et al. (2014). An in situ study of bioenergetic properties of human colorectal cancer: the regulation of mitochondrial respiration and distribution of flux control among the components of ATP synthasome. *Int. J. Biochem. Cell Biol.* **55**, 171–186.
- Katt, W.P., Ramachandran, S., Erickson, J.W., and Cerione, R.A. (2012). Dibenzophenanthridines as inhibitors of glutaminase C and cancer cell proliferation. *Mol. Cancer Ther.* **11**, 1269–1278.
- Le, A., Lane, A.N., Hamaker, M., Bose, S., Gouw, A., Barbi, J., Tsukamoto, T., Rojas, C.J., Slusher, B.S., Zhang, H., et al. (2012). Glucose-independent glutamine metabolism via TCA cycling for proliferation and survival in B cells. *Cell Metab.* **15**, 110–121.
- Ling, H., Fabbri, M., and Calin, G.A. (2013a). MicroRNAs and other non-coding RNAs as targets for anticancer drug development. *Nat. Rev. Drug Discov.* **12**, 847–865.
- Ling, H., Spizzo, R., Atlasi, Y., Nicoloso, M., Shimizu, M., Redis, R.S., Nishida, N., Gafà, R., Song, J., Guo, Z., et al. (2013b). CCAT2, a novel noncoding RNA mapping to 8q24, underlies metastatic progression and chromosomal instability in colon cancer. *Genome Res.* **23**, 1446–1461.
- Lutz, C.S., and Moreira, A. (2011). Alternative mRNA polyadenylation in eukaryotes: an effective regulator of gene expression. *Wiley Interdiscip. Rev. RNA* **2**, 23–31.
- Lyubchenko, Y.L., Shlyakhtenko, L.S., and Ando, T. (2011). Imaging of nucleic acids with atomic force microscopy. *Methods* **54**, 274–283.
- Masamha, C.P., Xia, Z., Yang, J., Albrecht, T.R., Li, M., Shyu, A.B., Li, W., and Wagner, E.J. (2014). CFIm25 links alternative polyadenylation to glioblastoma tumour suppression. *Nature* **510**, 412–416.
- Mercer, T.R., Dinger, M.E., and Mattick, J.S. (2009). Long non-coding RNAs: insights into functions. *Nat. Rev. Genet.* **10**, 155–159.
- Millevoi, S., Loulergue, C., Dettwiler, S., Karaa, S.Z., Keller, W., Antoniou, M., and Vagner, S. (2006). An interaction between U2AF 65 and CF Im links the splicing and 3' end processing machineries. *EMBO J.* **25**, 4854–4864.
- Naganuma, T., Nakagawa, S., Tanigawa, A., Sasaki, Y.F., Goshima, N., and Hirose, T. (2012). Alternative 3'-end processing of long noncoding RNA initiates construction of nuclear paraspeckles. *EMBO J.* **31**, 4020–4034.
- Nagasaki, H., Arita, M., Nishizawa, T., Suwa, M., and Gotoh, O. (2006). Automated classification of alternative splicing and transcriptional initiation and construction of visual database of classified patterns. *Bioinformatics* **22**, 1211–1216.
- Orengo, J.P., Bundman, D., and Cooper, T.A. (2006). A bichromatic fluorescent reporter for cell-based screens of alternative splicing. *Nucleic Acids Res.* **34**, e148.
- Rathore, M.G., Saumet, A., Rossi, J.F., de Bettignies, C., Tempé, D., Lecellier, C.H., and Villalba, M. (2012). The NF- κ B member p65 controls glutamine metabolism through miR-23a. *Int. J. Biochem. Cell Biol.* **44**, 1448–1456.
- Redis, R.S., Sieuwerts, A.M., Look, M.P., Tudoran, O., Ivan, C., Spizzo, R., Zhang, X., de Weerd, V., Shimizu, M., Ling, H., et al. (2013). CCAT2, a novel long non-coding RNA in breast cancer: expression study and clinical correlations. *Oncotarget* **4**, 1748–1762.
- Stine, Z.E., Walton, Z.E., Altman, B.J., Hsieh, A.L., and Dang, C.V. (2015). MYC, Metabolism, and Cancer. *Cancer Discov.* **5**, 1024–1039.
- Tian, B., Pan, Z., and Lee, J.Y. (2007). Widespread mRNA polyadenylation events in introns indicate dynamic interplay between polyadenylation and splicing. *Genome Res.* **17**, 156–165.
- Tomlinson, I., Webb, E., Carvajal-Carmona, L., Broderick, P., Kemp, Z., Spain, S., Penegar, S., Chandler, I., Gorman, M., Wood, W., et al.; COGRI Consortium (2007). A genome-wide association scan of tag SNPs identifies a susceptibility variant for colorectal cancer at 8q24.21. *Nat. Genet.* **39**, 984–988.
- Tuupainen, S., Turunen, M., Lehtonen, R., Hallikas, O., Vanharanta, S., Kivioja, T., Björklund, M., Wei, G., Yan, J., Niittymäki, I., et al. (2009). The common colorectal cancer predisposition SNP rs6983267 at chromosome 8q24 confers potential to enhanced Wnt signaling. *Nat. Genet.* **41**, 885–890.
- van den Heuvel, A.P., Jing, J., Wooster, R.F., and Bachman, K.E. (2012). Analysis of glutamine dependency in non-small cell lung cancer: GLS1 splice variant GAC is essential for cancer cell growth. *Cancer Biol. Ther.* **13**, 1185–1194.
- Vander Heiden, M.G. (2011). Targeting cancer metabolism: a therapeutic window opens. *Nat. Rev. Drug Discov.* **10**, 671–684.
- Wang, J., Liu, X., Wu, H., Ni, P., Gu, Z., Qiao, Y., Chen, N., Sun, F., and Fan, Q. (2010a). CREB up-regulates long non-coding RNA, HULC expression through interaction with microRNA-372 in liver cancer. *Nucleic Acids Res.* **38**, 5366–5383.
- Wang, J.B., Erickson, J.W., Fuji, R., Ramachandran, S., Gao, P., Dinavahi, R., Wilson, K.F., Ambrosio, A.L., Dias, S.M., Dang, C.V., and Cerione, R.A.

- (2010b). Targeting mitochondrial glutaminase activity inhibits oncogenic transformation. *Cancer Cell* 18, 207–219.
- Warburg, O., Posener, K., and Negelein, E. (1924). Über den Stoffwechsel der Carcinomzelle. *Biochem. Zeitschr* 152, 309–344.
- Ward, P.S., and Thompson, C.B. (2012). Metabolic reprogramming: a cancer hallmark even warburg did not anticipate. *Cancer Cell* 21, 297–308.
- Wilusz, J.E., Sunwoo, H., and Spector, D.L. (2009). Long noncoding RNAs: functional surprises from the RNA world. *Genes Dev.* 23, 1494–1504.
- Xia, Z., Donehower, L.A., Cooper, T.A., Neilson, J.R., Wheeler, D.A., Wagner, E.J., and Li, W. (2014). Dynamic analyses of alternative polyadenylation from RNA-seq reveal a 3'-UTR landscape across seven tumour types. *Nat. Commun.* 5, 5274.
- Yang, Q., Gilmartin, G.M., and Doublé, S. (2011). The structure of human cleavage factor I(m) hints at functions beyond UGUA-specific RNA binding: a role in alternative polyadenylation and a potential link to 5' capping and splicing. *RNA Biol.* 8, 748–753.
- Yang, F., Zhang, H., Mei, Y., and Wu, M. (2014). Reciprocal regulation of HIF-1 α and lincRNA-p21 modulates the Warburg effect. *Mol. Cell* 53, 88–100.
- Yoon, J.H., Srikantan, S., and Gorospe, M. (2012). MS2-TRAP (MS2-tagged RNA affinity purification): tagging RNA to identify associated miRNAs. *Methods* 58, 81–87.
- Zhou, Z., Licklider, L.J., Gygi, S.P., and Reed, R. (2002). Comprehensive proteomic analysis of the human spliceosome. *Nature* 419, 182–185.